AIP | Journal of Applied Physics

Efficient simulation of silicon nanowire field effect transistors and their scaling behavior

Mincheol Shin

Citation: J. Appl. Phys. **101**, 024510 (2007); doi: 10.1063/1.2430786
View online: http://dx.doi.org/10.1063/1.2430786
View Table of Contents: http://jap.aip.org/resource/1/JAPIAU/v101/i2
Published by the American Institute of Physics.

Efficient simulation of silicon nanowire field effect transistors and their scaling behavior

Mincheol Shin[a)]
School of Engineering, Information and Communications University, Daejeon 305-732, Republic of Korea

(Received 28 July 2006; accepted 17 November 2006; published online 23 January 2007)

We have simulated silicon nanowire field effect transistors in the ballistic transport regime using the effective mass theory and the mode space nonequilibrium Green's function method. In order to solve the two-dimensional Schrödinger equations on the nanowire cross-sectional planes as a part of the numerical procedure, we have developed an efficient numerical scheme, the product-space method, where the size of the eigenvalue problem is reduced to the number of subband modes that participate in the transport. We have investigated the scaling behavior of the nanowire transistors and found that their device characteristics sensitively depend on the aspect ratio of the channel length and width.
 [DOI: 10.1063/1.2430786]

I. INTRODUCTION

As the channel lengths of conventional planar metal oxide semiconductor field effect transistors (MOSFETs) shrink into the nanometer regime, performance of the devices becomes degraded mainly due to the short channel effects. Multiple gates around the channel of the silicon nanowire field effect transistors (SNWFETs) can improve the gate control considerably, and thus the short channel effects can be suppressed significantly. In addition, the SNWFETs show excellent current drive and have the merit of compatibility with conventional complimentary metal oxide semiconductor (CMOS) processes. The SNWFETs are therefore considered to be promising candidates for the next generation transistors and have drawn considerable attention recently.[1–3]

In a simulation of the SNWFETs, accurate modeling and calculations based on quantum mechanics are necessary to assess their performance limits, because the SNWFETs are expected to be a few nanometers wide in their ultimate scaling. There have been previous quantum mechanical simulations of the SNWFETs based on the effective mass theory (EMT) and the nonequilibrium Green's function (NEGF) formalism. Ballistic transport[4,5] and diffusive transport using the Büttiker probe model[4] have been considered, and the surface roughness scattering effect[6] has been investigated. There have also been works on the validity of using the simple EMT in simulations of the SNWFETs,[7,8] where it has been concluded that the EMT starts to be incorrect below the nanowire cross-sectional area of about 5×5 nm^2, but through the tuning of device parameters, the EMT can still be used below it.

The approach in this work is similar to the previous works mentioned above: we have used the EMT to model the device, because it has the merit of computational simplicity, and assumed ballistic transport. In our work, the product-space method was developed to efficiently solve the two-dimensional Schrödinger equations in the nanowire cross-sectional planes, and a scaling behavior of the SNWFETs has been investigated, paying attention to the dependence of the device characteristics on the aspect ratio of the channel length and width.

II. APPROACH

The device that we have considered in this work is a three-dimensional field effect transistor with source/drain, channel, and multiple gates as shown in Fig. 1. The source/drain is modeled as semi-infinite wires, which are heavily *n*-doped silicon, and the nanowire channel is assumed to be intrinsic or lightly *p*-doped silicon with a rectangular cross section. To simulate the device, we have self-consistently solved the three-dimensional Poisson equation with the ballistic transport equation expressed by the uncoupled mode space NEGF formalism[4,9] as follows.

The effective mass Hamiltonian of the device that we have used in our simulation is given by

$$H_{3D}\Psi(x,y,z) = E\Psi(x,y,z), \tag{1}$$

where

$$H_{3D} = -\frac{\hbar^2}{2m_x^*}\frac{\partial^2}{\partial x^2} - \frac{\hbar^2}{2m_y^*}\frac{\partial^2}{\partial y^2} - \frac{\hbar^2}{2m_z^*}\frac{\partial^2}{\partial z^2} + V(x,y,z), \tag{2}$$

where m_x^*, m_y^*, and m_z^* are effective masses and $V(x,y,z)$ is the conduction band edge profile. The wave function $\Psi(x,y,z)$ can be written as

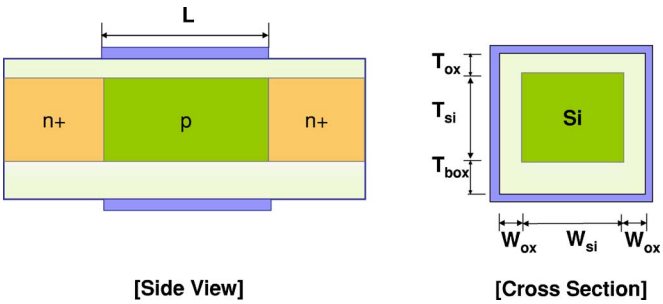

FIG. 1. Silicon nanowire field effect transistor.

[a)]Electronic mail: mcshin@icu.ac.kr.

$$\Psi(x,y,z) = \sum_m \varphi_m(x)\psi_m(y,z;x), \tag{3}$$

where $\psi_m(y,z;x)$ is the mth mode eigenfunction of the two-dimensional (2D) Schrödinger equation in the cross-sectional plane located at x, which is given by

$$H^{2D}\psi_m(y,z;x) = E_m(x)\psi_m(y,z;x), \tag{4}$$

where

$$H^{2D} = -\frac{\hbar^2}{2m_y^*}\frac{\partial^2}{\partial y^2} - \frac{\hbar^2}{2m_z^*}\frac{\partial^2}{\partial z^2} + V(y,z;x). \tag{5}$$

In the uncoupled mode space approach, coupling between different modes is ignored and $\varphi_m(x)$ of Eq. (3) satisfies[4]

$$\left[-\frac{\hbar^2}{2m_x^*}\frac{d^2}{dx^2} + E_m(x)\right]\varphi_m(x) = E\varphi_m(x). \tag{6}$$

In our simulation, the one-dimensional (1D) transport equation was solved by using the NEGF method: the 1D Green's function for subband m is given by

$$G_m = (E - H_m^{1D} - \Sigma_{S,m} - \Sigma_{D,m})^{-1}, \tag{7}$$

where H_m^{1D} is the 1D Hamiltonian in Eq. (6) and $\Sigma_{S,m}$ and $\Sigma_{D,m}$ are self-energies of the source (S) and drain (D). The 1D charge density $n_m^{1D}(x)$ is obtained via

$$n_m^{1D}(x) = \frac{1}{2\pi\Delta x}\int dE(f_S G_m \Gamma_{S,m} G_m^\dagger + f_D G_m \Gamma_{D,m} G_m^\dagger), \tag{8}$$

where Δx is the 1D lattice spacing, $f_{S,D}$ are the source and drain Fermi distribution functions, respectively, and

$$\Gamma_{S,m} = i(\Sigma_{S,m} - \Sigma_{S,m}^\dagger), \tag{9}$$

$$\Gamma_{D,m} = i(\Sigma_{D,m} - \Sigma_{D,m}^\dagger). \tag{10}$$

The three-dimensional (3D) quantum charge density is then calculated as

$$n^{3D}(x,y,z) = \sum_{m=1}^{M} n_m^{1D}(x)|\psi_m(y,z;x)|^2, \tag{11}$$

where M is the number of subbands participating in the transport, which is used in Poisson's equation,

$$\nabla^2\phi(x,y,z) = -\frac{q}{\epsilon}[N_D - n^{3D}(x,y,z)], \tag{12}$$

to be solved for the potential $\phi(x,y,z)$, where N_D is the doping concentration. Equations are solved iteratively until the self-consistent potential and charge distributions are obtained. If the self-consistency is reached, the current is calculated by using the Landauer-Büttiker formula,

$$I_d = \frac{2q}{h}\int dE T(E)[f_S(E) - f_D(E)], \tag{13}$$

where the transmission probability $T(E)$ is given by

$$T(E) = \sum_{m=1}^{M} \mathrm{Tr}(\Gamma_{S,m} G_m \Gamma_{D,m} G_m^\dagger). \tag{14}$$

III. SOLUTION OF 2D SCHRÖDINGER EQUATIONS IN THE PRODUCT SPACE

In this work, we have developed an efficient way to solve the 2D Schrödinger equations in the cross-sectional planes as follows. We write $\psi_m(y,z) \equiv \psi_m(y,z;x)$ of Eq. (4) in terms of the "product-space" basis $|K\rangle$,

$$\psi_m(y,z) = \sum_K A_K|K\rangle, \tag{15}$$

where A_K's are expansion coefficients and

$$|K\rangle \equiv \chi_i(y)\zeta_j(z). \tag{16}$$

In the above equation, $\chi_i(y) \equiv \chi_i(y;x)$ is the ith mode eigenfunction in the y direction with its eigenvalue $\epsilon_i^{(y)} \equiv \epsilon_i^{(y)}(x)$, satisfying

$$\left[-\frac{\hbar^2}{2m_y^*}\frac{d^2}{dy^2} + \bar{V}(y)\right]\chi_i(y) = \epsilon_i^{(y)}\chi_i(y), \tag{17}$$

where $\bar{V}(y) \equiv \bar{V}(y;x)$ is an average potential in the y direction, defined by

$$\bar{V}(y;x) = \frac{1}{T_{Si}}\int_{T_{ox}}^{T_{ox}+T_{Si}} dz V(x,y,z), \tag{18}$$

where T_{Si} is the depth of the silicon channel as shown in Fig. 1. Similarly, we define $\zeta_j(z) \equiv \zeta_j(z;x)$ as the jth mode eigenfunction in the z direction with its eigenvalue $\epsilon_j^{(z)} \equiv \epsilon_j^{(z)}(x)$, satisfying

$$\left[-\frac{\hbar^2}{2m_z^*}\frac{d^2}{dz^2} + \bar{V}(z)\right]\zeta_j(z) = \epsilon_j^{(z)}\zeta_j(z), \tag{19}$$

where $\bar{V}(z) \equiv \bar{V}(z;x)$ is an average potential in the z directions, defined by

$$\bar{V}(z;x) = \frac{1}{W_{Si}}\int_{W_{ox}}^{W_{ox}+W_{Si}} dy V(x,y,z). \tag{20}$$

The 1D eigenvalue problems of Eqs. (17) and (19) can be solved easily: using the finite difference discretization scheme and the 1D k-space transformation[10] expressed by

$$\chi_i(y) = \sum_m a_m(i)|m\rangle, \tag{21}$$

$$\zeta_j(z) = \sum_n b_n(j)|n\rangle, \tag{22}$$

where $|m\rangle$ and $|n\rangle$ are 1D k-space bases in each direction, respectively, and $a_m(i)$ and $b_n(j)$ are coefficients, the 1D eigenvalue problems can be solved in less than one-tenth of a second. If we use a uniform mesh of sizes N_y and N_z in the y and z directions, respectively, the index i in Eq. (17) will range from 1 to N_y, while j from 1 to N_z. K thus ranges from 1 to N_yN_z and we index it in the order of increasing value of the sum $\epsilon_i^{(y)} + \epsilon_j^{(z)}$.

If we put Eq. (15) into Eq. (4) and using the relationships of Eqs. (16)–(20), Eq. (4) is written as

$$\sum_K [\epsilon_K + V(y,z) - \bar{V}(y) - \bar{V}(z)]A_K|K\rangle = E_m \sum_K A_K|K\rangle, \tag{23}$$

where

$$\epsilon_K \equiv \epsilon_i^{(y)} + \epsilon_j^{(z)}. \tag{24}$$

Multiplying $\langle L|$ to the left of Eq. (23), we obtain

$$\sum_{K=1}^{N_y N_z} V_{LK} A_K = E_m A_L \quad (L = 1, \ldots, N_y N_z), \tag{25}$$

where

$$V_{LK} = \epsilon_L \delta_{LK} + \langle L|(V(y,z) - \bar{V}(y) - \bar{V}(z)\ )|K\rangle, \tag{26}$$

which is an eigenvalue problem and can be numerically solved using standard eigenvalue routines.

Notice that writing $\psi_m(y,z)$ as in Eqs. (15) and (16) is just another basis transformation: the size of the resultant matrix $\{V_{LK}\}$ in Eq. (26) is $N_y N_z \times N_y N_z$, which is of course the same size as the matrices that would have been obtained in the real-space or in the k-space representations. If we assess the performance of solvers in different representations by the size of the resulting matrices, we have gained nothing by the above transformation. However, in obtaining the eigenvalues and eigenfunctions in the nanowire cross-sectional planes, the product-space basis transformation turns out to be very useful, as will be discussed in the following.

First, we have found that, in solving the eigenvalue problem of Eq. (25), only the first $M \times M$ elements are sufficient, where M, as defined earlier, is the number of the subbands that contribute to the transport,

$$\sum_{K=1}^{M} V_{LK} A_K = E_m A_L \quad (L = 1, \ldots, M). \tag{27}$$

The eigenfunctions $\psi_m(y,z)$, $m=1,\ldots,M$, can be easily constructed from the eigenfunctions $\{A_K\}$. [Note that the uncoupled mode space NEGF approach that we have adopted in this work also requires only the first M modes in the transport part of the solution procedure, as seen in Eqs. (11) and (14).] For a specific example, let us consider a nanowire transistor of a cross-sectional area of 5×5 nm^2. Due to the strong quantum confinement in the transverse direction, subbands in the channel are well separated from one another energy wise and only the lowest ten subbands are sufficient to be considered in the transport, i.e., $M=10$ in this case. If we take a coarse mesh of size $N_y = N_z = 32$ in a k-space solution, the problem reduces to finding ten eigenvalues (and eigenfunctions) from a matrix of size 1024×1024. In our product-space method, however, we need to find ten eigenvalues (and eigenfunctions) from a matrix of size 10×10, so the computational burden of handling a large-size matrix is greatly reduced. Notice that M increases in proportion to the area S of the cross-sectional planes, as shown in Table I. Even for a nanowire transistor of rather large cross-sectional area, the resultant matrix size in our product-space solution is only a few hundreds by a few hundreds, which can be handled easily numerically.

TABLE I. Dependence of the number M of subband modes contributing to the transport and the band size N_B of the matrix $\{V_{LK}\}$ on the nanowire cross-sectional area S.

S (nm^2)	M	N_B
5×5	10	1
10×10	40	2
20×20	160	10
30×30	360	25

Second, we have found that the matrix $\{V_{LK}\}$ of Eqs. (25) and (26) is, in an excellent approximation, a banded matrix of band size N_B as shown in Fig. 2. N_B depends on the area S as shown in Table I. For example, if $S = 5 \times 5$ nm^2, $N_B = 1$. But if we neglect the possible degeneracy in ϵ_K's in Eq. (24), N_B is 0 in this case, i.e., the matrix $\{V_{LK}\}$ are practically diagonal,

$$V_{LK} = V_{KK} \delta_{LK}, \tag{28}$$

and the energy eigenvalues are simply given by

$$E_K = \epsilon_K + V_{KK}. \tag{29}$$

If S is increased, the off-diagonal elements near the diagonal elements gradually become significant: for $S \simeq 10 \times 10$ nm^2, up to the second off-diagonal elements from the diagonal elements should be also considered, and for $S \simeq 15 \times 15$ nm^2, up to the fifth off-diagonal elements from the diagonal elements should be included, and so on, as shown in Table I. The banded matrix nature of the matrix $\{V_{LK}\}$ has the effect of enhancing the computational efficiency of the product-space method.

To demonstrate the accurateness of our product-space method, we have compared a few eigenvalues from the product-space method and from the k-space method in Table II, for a nanowire transistor of $L = T_{Si} = W_{Si} = 10$ nm, $t_{ox} = 1$ nm, and with the drain and gate voltages of 0.5 and 1.5 V, respectively. M and N_B used in the product-space method are 40 and 2, respectively. The relative errors be-

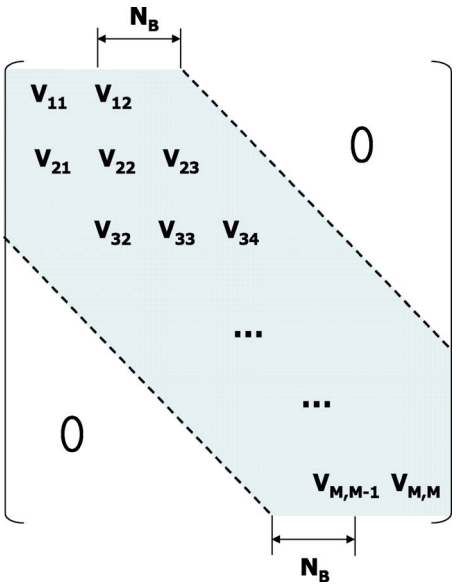

FIG. 2. The banded matrix $\{V_{LK}\}$.

TABLE II. Comparison of eigenvalues from the k-space solution and from the product-space solution. See the legend of Fig. 3 for the device parameters.

No.	Product space	k-space	Relative error
1	−0.203 02	−0.203074	0.000 25
2	−0.175 75	−0.175 77	0.000 10
3	−0.160 92	−0.160 95	0.000 17
4	−0.151 28	−0.151 35	0.000 41
5	−0.137 63	−0.137 67	0.000 33
6	−0.123 61	−0.123 63	0.000 19
7	−0.108 76	−0.108 80	0.000 32
8	−0.106 53	−0.106 59	0.000 57
9	−0.085 49	−0.085 55	0.000 62
10	−0.067 95	−0.068 04	0.001 30
⋮	⋮	⋮	⋮
31	0.158 99	0.158 78	0.001 37
32	0.170 91	0.170 72	0.001 09
33	0.194 67	0.194 53	0.000 74
34	0.211 16	0.210 92	0.001 14
35	0.216 18	0.216 06	0.000 56
36	0.231 29	0.231 07	0.000 99
37	0.233 70	0.233 44	0.001 13
38	0.240 60	0.240 42	0.000 75
39	0.244 72	0.244 66	0.000 27
40	0.259 56	0.259 48	0.000 33

tween the eigenvalues from the two solution methods are less than 10^{-3}. The first three wave functions from the two methods are compared in Fig. 3, where one can see excellent agreements between the solutions from the two methods.

Let us briefly explain why the product-space method is so successful in solving the 2D Schrödinger equations in the cross-sectional planes of the nanowire transistors. If one examines the second term in Eq. (26), one can see that the modified potential,

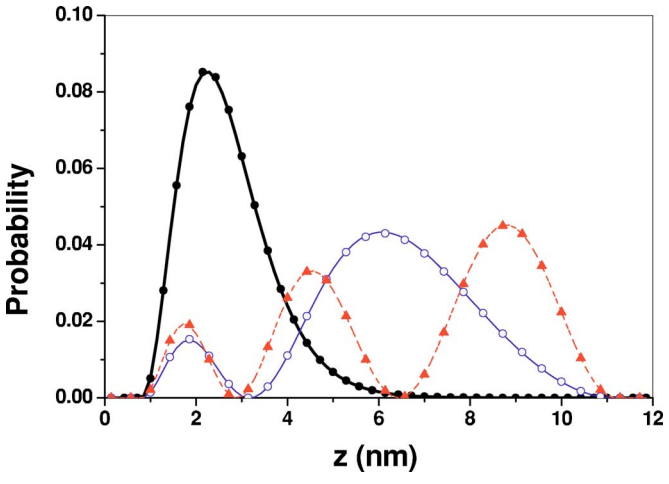

FIG. 3. The lowest three wave functions from the k-space solution (lines) and from the product-space solution (symbols), for the nanowire transistor of $L=T_{Si}=W_{Si}=10$ nm and $t_{ox}=1$ nm. The applied voltages are 0.5 and 1.5 V for drain and gate voltages, respectively, and the top-gate configuration is assumed. The wave functions were obtained on the cross-sectional plane located at the center of the channel, and their values in the z direction along the middle line ($y=6$ nm) are shown.

$$V(y,z) - \bar{V}(y) - \bar{V}(z), \tag{30}$$

gives the effect of making a mound-shaped potential profile into a much flattened one. In a transistor with a small cross-sectional area of 5×5 nm^2, for instance, the gate electric fields make the electron densities to be focused near the center of the cross-sectional plane, leading to a mound-shaped potential profile $V(y,z)$ formed in the middle of the plane. Therefore, the modified potential in Eq. (30) will be almost constant in this case, making only the diagonal terms in the matrix $\{V_{LK}\}$ to be nonzero. Considering the way that K is indexed, one may see that the eigenenergies should be given as in Eq. (29). As the area of the cross-sectional plane becomes larger, electron transport near the edges or corners of the silicon body gradually increases. As a consequence, potential profiles gradually develop near the interfaces between the silicon and oxide, giving rise to more nonzero off-diagonal terms in $\{V_{LK}\}$. The fact that the size of the matrix $\{V_{LK}\}$ is effectively reduced to $M\times M$ as in Eq. (27) also has much to do with the shape of the potential on the cross-sectional plane that has been just described. Note that the potentials in the 1D Schrödinger equations as defined in Eqs. (18) and (20) are the averaged ones in the silicon part of the plane. Since the conduction band profile in the oxide region is about 4 eV higher, in the case of silicon oxide, than that of the silicon region, the averaged potential will be obscured by the high conduction band profile of oxide if the oxide region is included in the averaging, leading to requiring more elements in the matrix $\{V_{LK}\}$.

A drawback in the product-space method is that elements V_{LK} of Eq. (26) need to be numerically evaluated, and it turns out that this part takes most of the computation time in the product-space solution. Note that, in the k-space method, the matrix elements can be computed very efficiently through the fast Fourier transformation,[10] which is not applicable in the product-space method. Nevertheless, the overall computation time of the product-space method is more than ten times, in a conservative estimation, faster than the k-space method. In Ref. 4, the so-called fast uncoupled mode space (FUMS) method has been introduced, where only one Schrödinger equation with a potential profile averaged over the cross-sectional planes is needed to be solved, thereby enabling a great improvement in the computational efficiency. Our product-space method is complimentary to the FUMS method, in the sense that ours is to accelerate calculations in one cross-sectional plane. Therefore, the product-space method can be combined with the FUMS method for even greater computational efficiency. Note, however, that the FUMS method can be applied to the uncoupled mode space approach only, because the wave functions are assumed to be identical on each of the cross-sectional planes in the FUMS method, whereas our product-space method can be applied to the coupled mode space approach as well, because the Schrödinger equations on cross-sectional planes are independently solved in the product-space method (our work in this paper, nonetheless, employs the uncoupled mode space approach for the transport calculation).

In this section, the product-space method has been described with the assumption that the effective masses are the

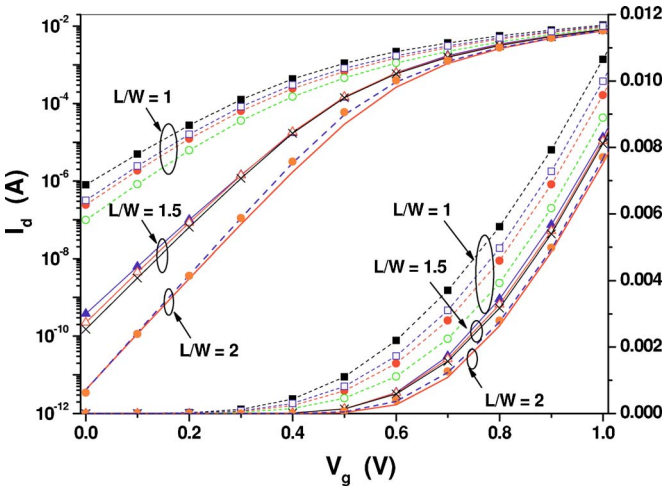

FIG. 4. I_d-V_g characteristics of GAA nanowire transistors (left: log scale, right: linear scale). The dotted lines represent $L/W=1$, where $W=5$ (solid squares), 8 (open squares), 10 (solid circles), and 15 nm (open circles), and thin sold lines $L/W=1.5$, where $W=5$ (solid triangles), 8 (open triangles), and 10 nm (crosses). For $L/W=2$, data are shown for $W=5$ (solid line with no symbols), 8 (dashed line with no symbols), and 10 nm (solid circles with no connecting line).

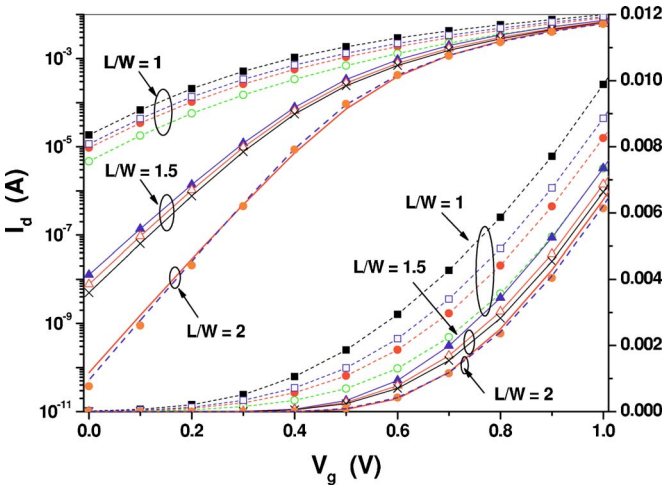

FIG. 5. I_d-V_g characteristics of trigate nanowire transistors (left: log scale, right: linear scale). See the caption of Fig. 4 for the legend.

same both in the silicon and oxide regions. It can be extended to include the mass discontinuity across the silicon-oxide interface with some reasonable approximations. We have found, however, that the effect of the mass discontinuity in the SNWFET simulations is almost negligible, as long as the final outcome of the simulation, the current-voltage characteristic, is concerned.

IV. SCALING BEHAVIOR

We now present results for the scaling behaviors of the SNWFETs with rectangular cross section, using the numerical schemes described in the previous sections. In the simulated devices, the source/drain are heavily n-doped with a doping concentration of 10^{20} cm^{-3}, the channel is intrinsic, and an abrupt doping profile is used. The silicon (100) orientation is parallel to the transport (x) direction. The gate oxide thickness is 1 nm, and metallic gates with the midgap work function are assumed.

In a scaling of ballistic SNWFETs, the general trend is that the device performance improves as the channel length L becomes longer (for the same cross-sectional area) or as the channel cross-sectional area $W \equiv W_{\mathrm{Si}}$ is decreased (for the same channel length), which we have confirmed in our simulations. In this work, we vary L and W simultaneously while the aspect ratio L/W is fixed. We have found as follows that the SNWFETs can be characterized by their aspect ratio.

Figure 4 shows the scaling behavior of the gate-all-around (GAA) transistors with square cross sections. Three aspect ratios of $L/W=1$, 1.5, and 2 were considered, and each of the aspect ratio simulations were done for three values of $W=5$, 8, and 10 nm. We first observe in the figure that the I-V_g characteristics of transistors of the same aspect ratio are more or less the same, and they are clearly distinguished from those of transistors of different aspect ratios. In particular, for $L/W=2$, subthreshold swing (SS) and $I_{\mathrm{on}}/I_{\mathrm{off}}$ remain almost the same regardless of the scaling. We next observe that the device performance strongly depends on the aspect ratio. Compared to the case of $L/W=1$, the device performance of transistors of $L/W=2$ is greatly improved. Notice that the SS approaches the theoretical limit of 60 mV/decade for $L/W=2$. The same trend is observed for the trigate transistors, as shown in Fig. 5: the current-voltage curves are clearly characterized by L/W and the device performance improves as L/W gets bigger.

Figure 6 shows the dependence of the SS values on the aspect ratio of the GAA transistors and trigate transistors considered in this work, respectively. For the same aspect ratio, the SS values of the trigate transistors are higher than those of the GAA transistors, which is logical since the GAA transistors have better gate control. It is noteworthy that the SS values increase rapidly with W/L and the rate of increase is higher for the trigate transistors. The inset of Fig. 6 shows that the SS values of transistors of the same aspect ratio are more or less the same with respect to the scaling, which is

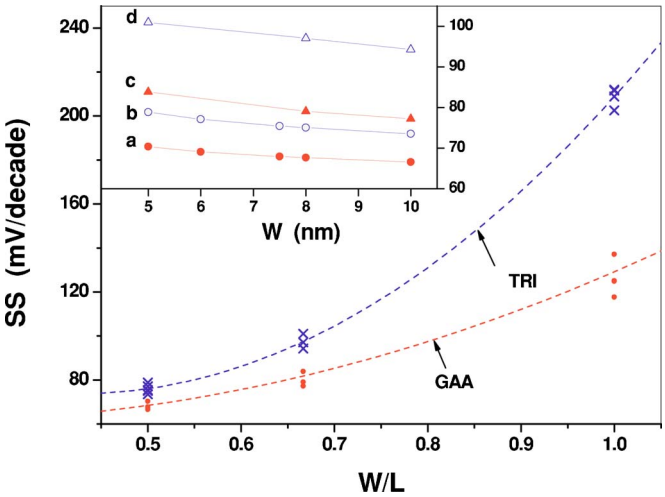

FIG. 6. SS values vs W/L for the GAA (solid circles) and trigate (crosses) transistors. The dashed lines are curves by the second order polynomial fitting. In the inset SS values vs W are shown, for the GAA transistor with $L/W=2$ (solid circles), the trigate transistor with $L/W=2$ (open circles), the GAA transistor with $L/W=1.5$ (solid triangles), and the trigate transistor with $L/W=1.5$ (open triangles).

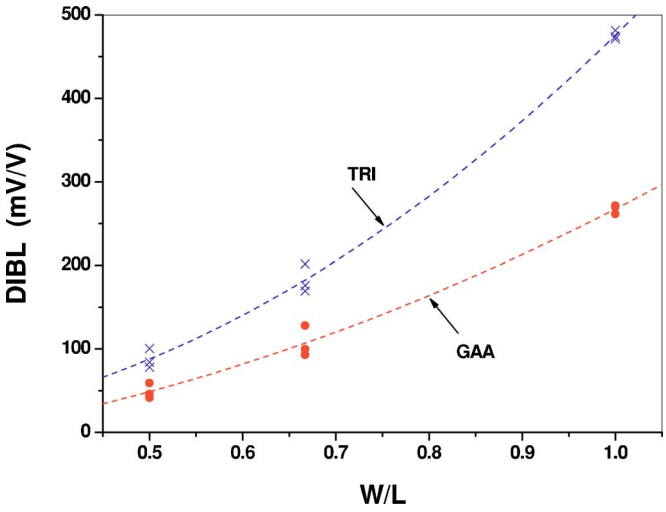

FIG. 7. DIBL vs W/L for the GAA (solid circles) and trigate (crosses) transistors. The dashed lines are curves by the second order polynomial fitting.

particularly true for transistors with higher aspect ratio. Similar behaviors are observed in Fig. 7, where the dependence of the drain induced barrier lowering (DIBL) on the aspect ratio of the GAA transistors and trigate transistors, respectively, is shown.

Figure 6 suggests that L/W should be greater than about 1.2 and 1.5 for GAA and trigate transistors, respectively, so that the SS values are 100 mV/decade or below. On the other hand, L/W should be greater than about 1.5 and 2.0 for GAA and trigate transistors, respectively, so that the DIBL values are 100 mV/V or below. We remark that we have tried other gate types such as pi and omega gates and found that they show the same trend as mentioned above: their SS and DIBL values, in particular, fall between the two lines of Figs. 6 and 7, respectively.

V. CONCLUSIONS

Silicon nanowire field effect transistors in the ballistic transport regime have been simulated based on the effective mass theory and using the self-consistent Poisson-NEGF calculations. To solve the two-dimensional Schrödinger equations in the nanowire cross-sectional planes as part of the numerical procedure, the product-space method, where the product of two one-dimensional wave functions forms a basis set, has been developed and its performance has been compared to the k-space method. Due to the reduced size of the eigenvalue problem and the banded matrix nature of the resultant matrix, the product-space method shows a great advantage in numerical calculations. Using the numerical schemes developed in this work, the scaling behavior of the silicon nanowire field effect transistors has been investigated, and it has been found that their device characteristics sensitively depend on the aspect ratio of the channel length and the channel width.

ACKNOWLEDGMENT

This research was supported by the Ministry of Information and Communication, Korea, under the Information Technology Research Center (ITRC) support program supervised by the Institute of Information Technology Assessment (IITA).

[1] J. T. Park and J. P. Colinge, IEEE Trans. Electron Devices **49**, 2222 (2002).
[2] Y. Cui, Z. Zhong, D. Wang, W. Wang, and M. Lieber, Nano Lett. **3**, 149 (2003).
[3] H.-S. Philip Wong, Solid-State Electron. **49**, 755 (2005).
[4] J. Wang, E. Polizzi, and M. Lundstrom, J. Appl. Phys. **96**, 2192 (2004).
[5] M. Bescond, K. Nehari, J. L. Autran, N. Cavassilas, D. Munteanu, and M. Lannoo, Tech. Dig. - Int. Electron Devices Meet. **2004**, 617.
[6] J. Wang, E. Polizzi, A. Ghosh, S. Datta, and M. Lundstrom, Appl. Phys. Lett. **87**, 043101 (2005).
[7] J. Wang, A. Rahman, A. Ghosh, G. Klimeck, and M. Lundstrom, IEEE Trans. Electron Devices **52**, 1589 (2005).
[8] K. Nehari, N. Cavassilas, J. L. Autran, M. Bescond, D. Munteanu, and M. Lannoo, Proceedings of the 35th European Solid-State Device Research Conference, 2005 (ESSDERC, 2005), 12–16 Sept. 2005, pp. 229–232.
[9] S. Datta, Superlattices Microstruct. **28**, 253 (2000).
[10] A. Abramo, A. Cardin, L. Selmi, and E. Sangiorgi, IEEE Trans. Electron Devices **47**, 1858 (2000).